Version of Record: https://www.sciencedirect.com/science/article/pii/S0924271618302016
Manuscript_9deb7afc53702068cda0ff4ceffa162b

A self-adaptive approach for producing clear-sky composites from VIIRS surface reflectance datasets

Jinhu Bian[a,b,c], Ainong Li [a,*], Chengquan Huang[c,] , Rui Zhang[c], Xiwu Zhan[d]

[a] *Institute of Mountain Hazards and Environment, Chinese Academy of Sciences, Chengdu Sichuan 610041, China*

[b] *University of Chinese Academy of Sciences, Beijing 100049, China*

[c] *Department of Geographical Sciences, University of Maryland, College Park, MD 20742, USA*

[d] *Center for Satellite Applications and Research, NESDIS/NOAA, College Park, MD, USA*

Abstract: With the launch of the Joint Polar Satellite System (JPSS)/Soumi National Polar-orbiting Partnership (S-NPP) satellite in October 2011, the need for the operational monitoring of terrestrial processes at the regional and global scales led to the expansion of terrestrial remote sensing products (*e.g.*, the clear-sky composited surface reflectance products) generated from the Moderate Resolution Imaging Spectroradiometer (MODIS) into the JPSS/S-NPP mission using the new Visible Infrared Imaging Radiometer Suite (VIIRS) data. Seamless cloud composites are usually generated using a single criterion without an explicit consideration of phenological variations among different surface types. However, because the spectral signals of many surface types change dramatically due to seasonal variations, the single-criterion compositing methods are only effective for specific surface cover conditions. This study proposed a new self-adaptive compositing approach (SA-Comp) to produce global terrestrial clear-sky VIIRS surface reflectance composites. The proposed approach employs contextual spectral and temporal information to determine the surface cover conditions within a pre-defined temporal window, and adaptively selects the most suitable criterion. A comprehensive evaluation of the SA-Comp approach was conducted by comparing it with the maximum NDVI (MaxNDVI), minimum Red (MinRed) and maximum ratio (MaxRatio) compositing schemes, and with the MODIS and VIIRS composited surface reflectance products. The results, including visual representations and temporal profiles, revealed that the SA-Comp approach outperformed all of the other methods. The results also highlighted that the SA-Comp approach is more feasible and effective at compositing global VIIRS data and has great potential for regional, national and even global terrestrial monitoring.

Keywords: VIIRS, temporal compositing, adaptive, global, SA-Comp, clear-sky

1. Introduction

The launch of the Joint Polar Satellite System (JPSS)/Suomi National Polar-orbiting Partnership (S-NPP) mission in October 2011 marked a new generation of operational polar-orbiting spacecraft (Justice et al., 2013). It is well known that the Moderate Resolution Imaging Spectroradiometer (MODIS) instruments on board the Terra and Aqua satellites have far exceeded their initial design life (Cao et al., 2013). Consequently, the goal of the Visible Infrared Imaging Radiometer Suite (VIIRS) instrument on board the S-NPP is to improve upon the operational Advanced Very High Resolution Radiometer (AVHRR) and provide continuity with MODIS to provide global environmental measurements. The VIIRS instrument has a medium spatial resolution (375 and 750 m at nadir) and multispectral (22 bands) capabilities as well as visible capabilities for nighttime

© 2018 published by Elsevier. This manuscript is made available under the Elsevier user license
https://www.elsevier.com/open-access/userlicense/1.0/

imaging using the day/night band (DNB) (Zhang et al., 2017). Subsequent to the VIIRS first-light images acquired in November 2011, a suite of operational products (Niclòs et al., 2018), including environmental data records (EDRs), has been developed by scientists from the National Aeronautics and Space Administration (NASA) and the National Oceanic and Atmospheric Administration (NOAA).

The VIIRS sensor has a 3,040-km-wide swath. Consequently, the images obtained by VIIRS provide complete coverage of the Earth's surface without the spatial gaps between adjacent orbits in MODIS or AVHRR global mosaicked images (Hillger et al., 2013). However, due to the presence of cloud cover, sensor limitations and suboptimal imaging conditions, the time series images and EDR parameters extracted from VIIRS data still suffer from spatial and temporal discontinuity problems that have seriously restricted the application of VIIRS data to land surface process simulation, climate modeling and global climate change studies.

Based on different user-defined rules, image compositing can be employed to select the highest-quality observation over the same geographical region from multi-temporal images in a certain period to provide cloud-free and seamless images over large areas (Bian et al., 2015; Griffiths et al., 2013; Roy et al., 2010; Vermote and Vermeulen, 1999). Numerous compositing methods have been proposed to date for different applications, although each was designed with the purpose of optimally eliminating the influences of cloud cover, aerosols and various other factors (Bian et al., 2017; Dennison et al., 2007; Luo et al., 2008). The maximum value composite (MVC) method was first proposed by Holben (1986) and applied to the maximum normalized difference vegetation index (NDVI) for the compositing of multi-temporal AVHRR data. While it remains the most commonly utilized compositing algorithm, the MVC technique tends to select pixels from forward-scattering view geometries and does not work over water bodies (Luo et al., 2008). To avoid some of the problems associated with the MVC, several other methods that rely on low reflectance values in the visible wavelengths to discriminate clear pixels from cloud-contaminated pixels has been proposed (Chuvieco et al., 2005; Vermote and Vermeulen, 1999). These include methods that utilize minimum values in the blue or red band. Since these minimum reflectance methods may select cloud shadow pixels, some scholars suggested using the third-lowest value in the time series based on the assumed low likelihood of a cloud shadow occurring within a given pixel more than twice (Cabral et al., 2003). Image compositing for wide swath data must also consider large spectral distortions introduced by the bidirectional reflectance distribution function (BRDF). To mitigate this problem, some techniques employ view angle constraints to reduce the likelihood of selecting observations with extremely high view angles (Huete et al., 2002).

In addition to these single-criterion methods, multi-criteria methods have also been proposed (Chuvieco et al., 2005; Frantz et al., 2017; Griffiths et al., 2013; Luo et al., 2008; Roy et al., 2010). For example, the criteria matrix scheme was proposed to combine multiple criteria to produce MODIS clear-sky composites (Luo et al., 2008). Multi-criteria methods consider the spectral characteristics of the land surface and clouds in different wavelengths. Consequently, they are more effective than single-criterion methods in many cases (Chuvieco et al., 2005; Luo et al., 2008). However, multi-criteria methods often rely on cloud mask products (Frantz et al., 2017; Griffiths et al., 2013), which typically have errors and hence may lead to erroneous compositing results. In addition, although multi-criteria methods can utilize the multispectral properties of clouds and land surfaces, the phenological variations in the land surface are still not fully considered. When the surface of a target area changes dramatically within a single year, the temporal variation will result

in drastic spectral changes, leading to failure in some compositing cases. For instance, multi-criteria methods using only spectral information may fail for annual herbaceous vegetation or open water at high latitudes in the wintertime when the ground is covered by snow or ice over long periods of time.

The main goal of this work is to propose a new approach that can address the above problems in creating global clear view composites using VIIRS observations. The proposed approach employs temporal and spectral information using a two-level, self-adapted technique to determine the surface cover condition of each pixel during a specific time period, which is then used to select an appropriate compositing method for identifying a clear-sky observation during that time period. The approach was evaluated via a comprehensive comparison with three existing compositing methods, namely, the maximum NDVI (MaxNDVI) (Holben, 1986), minimum Red (MinRed) (Chuvieco et al., 2005) and maximum Ratio (MaxRatio) (Luo et al., 2008) methods, and with the MODIS MYD09A1 Collection 6 (Vermote et al., 2015) and VIIRS (Roger et al., 2016) VNP09A1 composited surface reflectance products at the regional and global scales. The global VIIRS compositing results were finally composited using the proposed approach.

2. Data and Processing

The VIIRS instrument is a critical payload onboard the S-NPP satellite. VIIRS has three types of bands: five high-resolution imagery bands (I-bands, with a nadir resolution of 375 m), 16 moderate resolution bands (M-bands, with a nadir resolution of 750 m), and the DNB (750-m resolution, near constant across scan). The M-bands are listed in Table 1.

Table 1. List of the VIIRS M-bands. The ones used in this study are highlighted in bold face*.

Band	Central Wavelength (μm)	Bandwidth (μm)	Wavelength Range (μm)	Band Explanation
M1*	0.412	0.02	0.402-0.422	Visible/Reflective
M2*	0.445	0.018	0.436-0.454	
M3*	0.488	0.02	0.478-0.488	
M4*	0.555	0.02	0.545-0.565	
M5*	0.672	0.02	0.662-0.682	
M6	0.746	0.015	0.739-0.754	Near IR
M7*	0.865	0.039	0.846-0.885	
M8*	1.24	0.020	1.23-1.25	Shortwave IR
M9	1.38	0.015	1.371-1.386	
M10*	1.61	0.06	1.58-1.64	
M11*	2.25	0.05	2.23-2.28	
M12	3.7	0.18	3.61-3.79	Mediumwave IR
M13	4.05	0.155	3.97-4.13	
M14	8.55	0.3	8.4-8.7	Longwave IR
M15	10.76	1.0	10.26-11.26	
M16	12.01	0.95	11.54-12.49	

The VIIRS surface reflectance intermediate product (IP) for 2015 from bands M1 to M11 (excluding M6 and M9) were obtained from the NOAA's Comprehensive Large Array-Data Stewardship System (CLASS) (NOAA, 2016). The standard VIIRS surface reflectance IP product is processed in NOAA's Interface Data Processing System and produced in swath-based format

(NOAA, 2014). The swath data were then reprojected into a sinusoidal projection and mosaicked into global daily data following the method described in Zhang et al. (2017). The dimensions of the global mosaicked images are 43,200 columns × 21,600 rows, and the spatial resolution is 926.65 m. The NDVI, normalized difference water index (NDWI) and normalized difference snow index (NDSI) were calculated from the equations provided in Table 2. These indices were useful for enhancing specific surface type signals in previous studies.

Table 2. Spectral indices used in conjunction with the VIIRS bands during the compositing.

Spectral Index	Formula	Reference
NDVI	$(\rho_{M7} - \rho_{M5}) / (\rho_{M7} + \rho_{M5})$	Tucker (1979)
NDWI	$(\rho_{M5} - \rho_{M10}) / (\rho_{M5} + \rho_{M10})$	Gao (1996)
NDSI	$(\rho_{M4} - \rho_{M10}) / (\rho_{M4} + \rho_{M10})$	Hall (1995)

3. Methodology

3.1 Existing single-criterion compositing methods

Many existing single-criterion clear-sky compositing methods utilize minimum or maximum rules, such as the MaxNDVI (Holben, 1986), MinRed (Chuvieco et al., 2005), median values (Flood, 2013) or some other single-threshold criterion to select clear-sky observations. These approaches are designed to screen clouds automatically because they often prefer clear-sky pixels over cloudy ones. For vegetated surfaces, for example, cloud contamination typically results in increased reflectance in the red band and decreased NDVI values. Therefore, either the MaxNDVI or MinRed method can select clear-sky observations over cloudy observations. When the surface is covered by water, however, the MaxNDVI method prefers cloudy observations over clear-sky water observations, because clouds typically have lower NDVI values than water. When the surface is covered by snow/ice, both MaxNDVI and MinRed could fail because snow/ice does not always have higher NDVI or lower red reflectance than clouds. Because cloud shadows typically have lower reflectance than clear-sky surfaces, the MinRed method often choses shadow observations when they are present. The minimum blue method has similar strengths and shortcomings as the MinRed method. A summary of the advantages and disadvantages of these and some other compositing methods is provided in Table 3.

Table 3. Descriptions of the existing single-criterion compositing algorithms

Composite abbreviation	Advantages	Shortages	Reference
MaxNDVI	Effective for selecting green vegetation	Selects cloudy pixels over water/snow surface	Holben (1986)
MinRed	Effective for excluding clouds	Cloud shadows will be selected	Chuvieco et al. (2005)
MaxRatio or [Max(NIR, SWIR)/Blue]	Effective for excluding cloud shadows	Not suitable for snow covered surfaces	Luo et al. (2008)
Multi-Dimensional Median	producing imagery which is representative of the time period	problematic for short time scales	Flood (2013)

3.2 The self-adaptive compositing method

3.2.1 The overall concept

The above discussion illustrates the need for using different methods to choose clear-sky observations when the surface cover conditions (SCCs) are different. When vegetation is present, the MaxNDVI method works well. When the surface is covered by water or snow/ice, other methods have to be used. Further, the SCC at a given location can change over time. A vegetated area loses the green leaves during the leaf-off season. Dry land areas can be covered by water when flooded, or by snow/ice during the winter. Surface water can be covered by snow/ice during the winter. In the self-adaptive compositing (SA-Comp) method, these SCCs and their change over time are considered explicitly in determining the appropriate method for selecting clear-sky observations. Therefore, this method has two major steps – determining the SCC at each pixel location during a specific compositing period and selecting an appropriate compositing method for that SCC. A flowchart of this method for generating monthly or sub-monthly (*e.g.*, 8-day, 16-day, 32-day) composites using daily observations is shown in Figure 1.

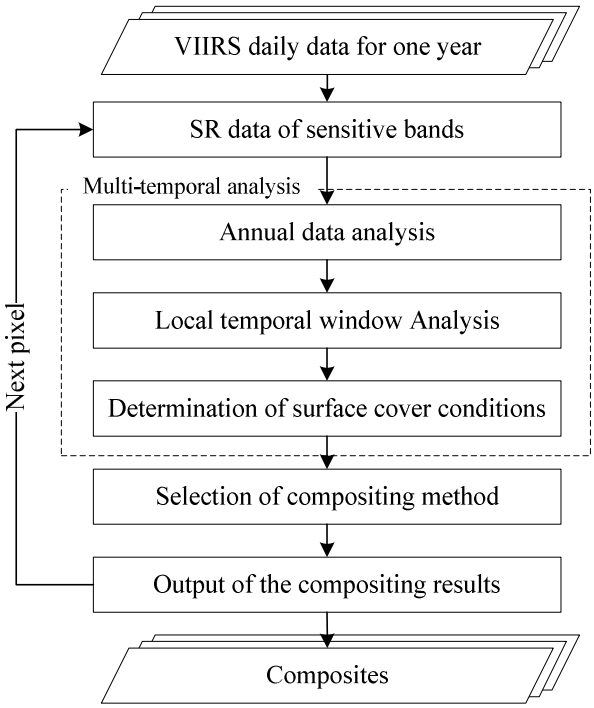

Figure 1. Flowchart of the proposed SA-Comp method.

3.2.2 Spectral characteristics of different SCCs

The SA-Comp method distinguishes four SCCs in choosing a suitable compositing method: green vegetation, water, snow/ice, and barren (including vegetated surfaces that don't have green canopy cover during the leaf-off season). To determine the spectral range and separability of these SCCs, we identified clear-sky samples for each of the four SCCs as well as cloud samples through visual examination of VIIRS daily data that had the least cloud cover in each of the 12 months of 2015. Boxplots of these samples in the red (M5), near infrared (M7), and shortwave infrared (M10) bands, as well as their NDVI, NDSI, and NDWI values are shown in Figure 2.

As expected, the clouds and snow/ice exhibit high reflectance values in visible and near-infrared (NIR) bands. However, snow and ice have a lower reflectance in the shortwave infrared (SWIR) band than most liquid clouds. Barren also has high reflectance values in the visible through the

SWIR bands, but it can separated from clouds, water, and snow/ice with negative NDWI values. Water pixels have low reflectance values in the NIR and SWIR bands and high NDWI values. Green vegetation pixels characteristically exhibit low reflectance values in the red band due to the strong absorption of photosynthetically active radiation and high reflectance in the NIR band due to strong reflection by chlorophyll in green leaves. They have high NDVI values and low NDWI values.

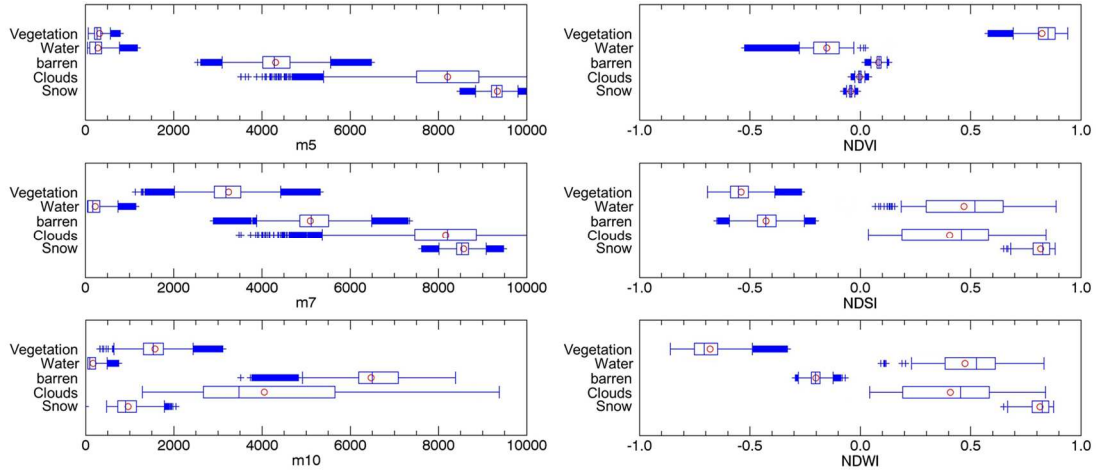

Figure 2. Boxplots of four surface cover conditions (SCCs) and clouds showing their median (vertical line), mean (red circle), as well as the lower and upper quartiles (lower and upper end of the each box) of the observed data ranges. The whiskers extend to the 1.5 interquartile range beyond the lower and upper quantiles. The blue crosses denote extreme outliers. Note that the scales for the spectral reflectance and spectral index are different.

3.2.3 Determining SCC with cloud presence using temporal statistics

The distinctive spectral characteristics of different SCCs under clear-sky conditions make it possible to separate them under cloudy conditions. Assuming the SCC at a pixel location does not change during a specific compositing period, the SCC can be determined based on observations from Figure 2 as long as there is at least one clear-sky observation during that compositing period. Unfortunately, without a good cloud mask product, which observations are clear-sky observations is unknown, in the SA-Comp method, a 2-tiered approach is used to determine the SCC based on temporal statistics derived from time series data that typically contain both clear-sky and cloudy observations.

In the first tier, annual time series data of a pixel are analyzed to determine its SCC on an annual basis using the following:

$$\text{SCC}=\begin{cases}\text{type 1}, & \text{CP}(SP_{yearly} \geq T_{\text{SP}}) \geq T_{\text{CP}} \\ \textit{Not}\ \text{type 1}, & \text{CP}(SP_{yearly} \geq T_{\text{SP}}) < T_{\text{CP}}\end{cases} \quad (1)$$

where CP is the cumulative percentage of observations that meet the conditional statement in the parentheses, SP is the value of a spectral band or index, T_{SP} is the threshold of SP, and T_{CP} is the threshold for CP. The goal of this tier is to determine whether a pixel had vegetation cover at least during some time of a year, and if not, whether it was covered by snow/ice or water year-round.

To determine the threshold values for T_{SP} and T_{CP}, we selected samples of different land cover types from across the globe according to a global surface type product based on 2015 VIIRS data

(Zhang et al., 2017). The samples were divided into two groups. One group included the surface types without apparent seasonal changes, including permanent water (PWT), permanent snow (PSN), barren land (BRL) and evergreen vegetation (EVG). The other group included types that have seasonal variations, including water bodies that may have snow and ice (WSI) on the surface during winter, deciduous vegetation (DVT) in tropical areas (i.e., deciduous forests, shrubs, herbaceous and croplands) that are not subject to snow cover and deciduous vegetation (DVN) in non-tropical areas that may be subject to snow cover during the winter. A summary of the selected samples is provided in Table 4. Their geographic distribution is illustrated in Figure 3.

Table 4. Numbers of samples for the typical surface types.

Main Surface type	Sub-classes	Explanation	Number of pixels
Water	PWT	permanent water body without ice or snow	1.66×10^7
	WSI	water samples with snow and ice during the winter	1.07×10^7
Permanent snow	PSN	Permanent snow or ice area such as the Greenland and glacier in high mountain regions	3.71×10^7
Barren land	BRL	Including bare soil, barren land, desert etc.	4.01×10^7
Vegetation	EVG	Evergreen shrubs, forests etc.	3.68×10^7
	DVT	Deciduous vegetation in tropical areas (i.e., where snow cover is unlikely during any time of the year). Including croplands, savannas, grassland, deciduous shrubs and forests.	3.69×10^7
	DVN	Deciduous vegetation in non-tropical areas (i.e., vegetation that may be subject to snow cover for parts of or throughout the entire year). Including croplands, grassland, deciduous shrubs and forests.	3.68×10^7

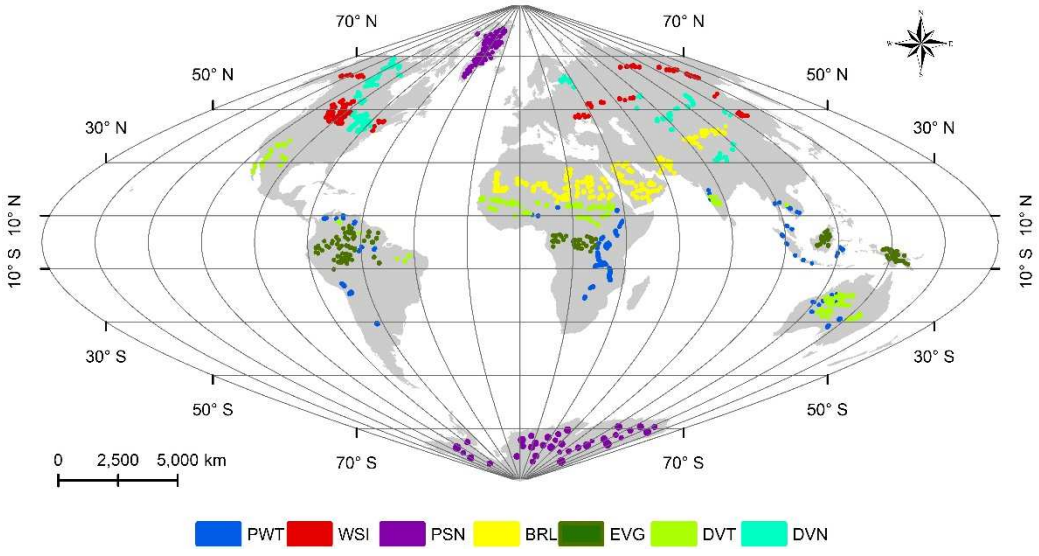

Figure 3. Geographical distribution of the samples for different surface types shown in 5 by 5 pixels. See the sub-classes in Table 4 for the surface type represented by each abbreviation)

For each selected sample, daily time series data that included both clear-sky observations and observations contaminated by cloud or shadow were extracted from the 2015 VIIRS surface reflectance product. Histograms and cumulative histograms were created using these samples for each of the surface types listed in Table 4 for the red (M5), NIR (M7), and SWIR (M10), as well as

NDVI, NDWI, and NDSI (Figure 4). As expected, the NDVI values of most samples (>95%) of the non-vegetated classes, including open water, barren land and permanent snow, were below 0.2 regardless of cloud or shadow contamination. Because the NDWI and NDSI values of clouds, water, and snow/ice are positive while those of vegetation and barren are negative (Figure 2), most samples (> 95%) of the open water and permanent snow classes have NDWI and NDSI values higher than 0 under both clear-sky and cloud/shadow conditions. The percentage of observations with negative NDWI and NDSI values increased substantially (>5%) for the classes that are not covered by water or snow/ice at least during part of a year.

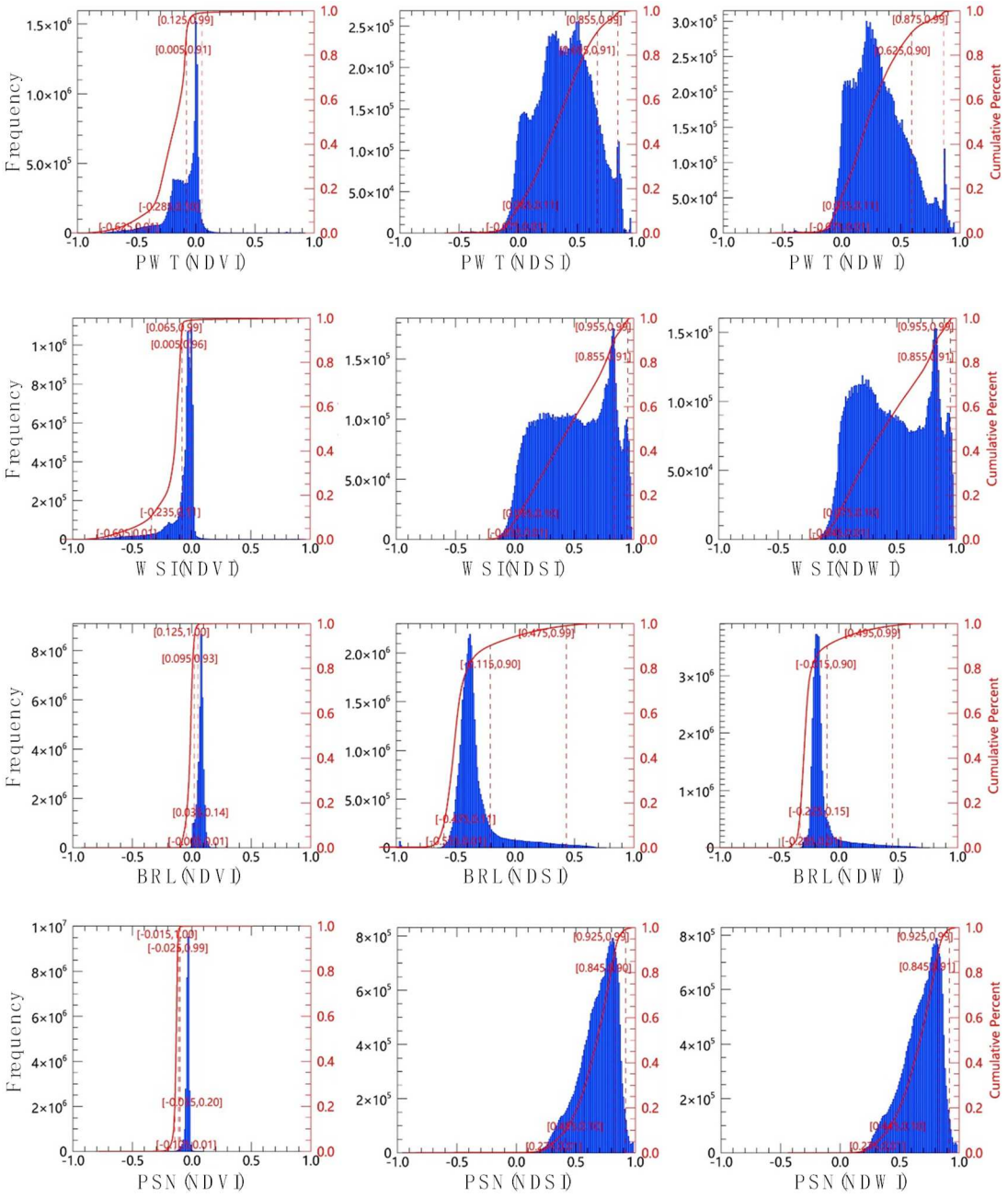

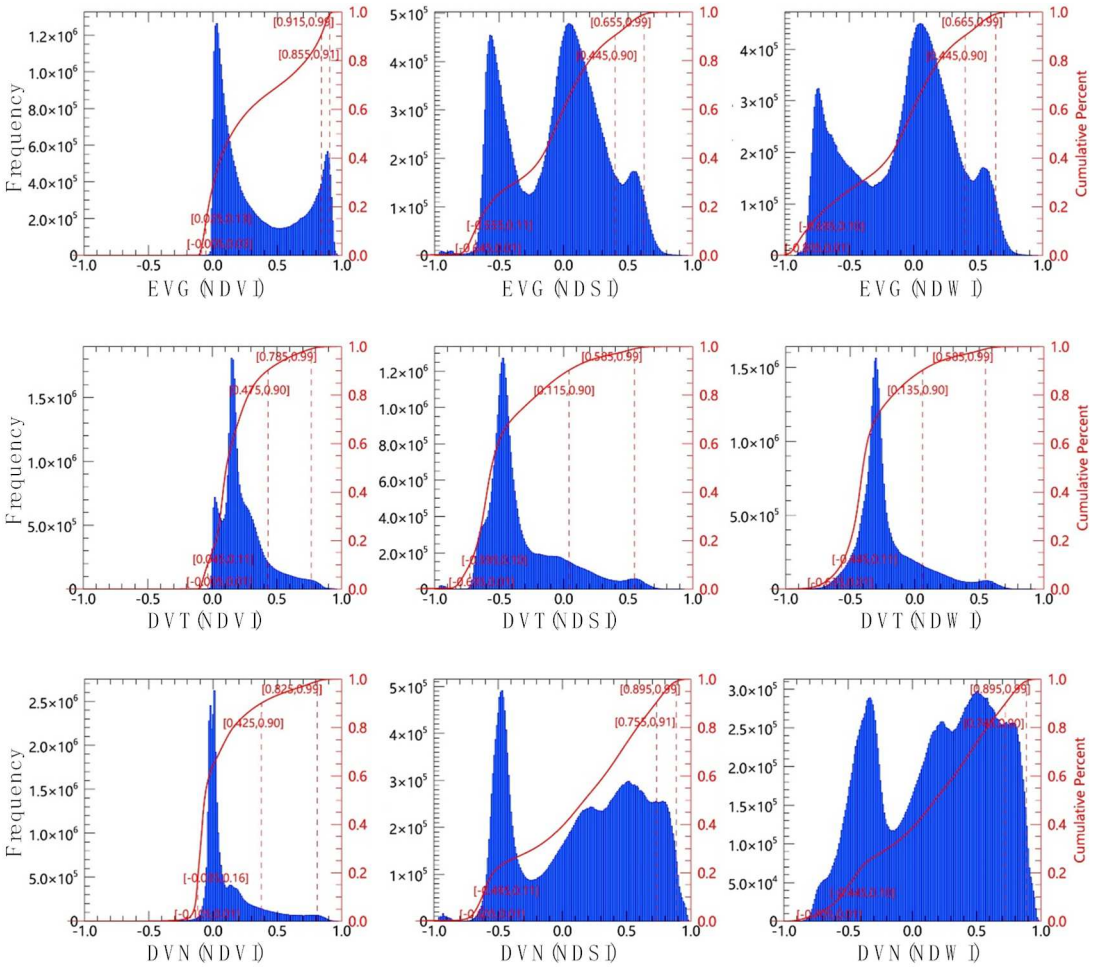

Figure 4. Histograms of the time series values of spectral indices for major surface types (represented by the 3-letter abbreviations in the caption for the x-axis; See the sub-classes in Table 4 for the surface type represented by each abbreviation) mixed with clouds.

For pixels covered by snow/ice or water year-round, a single compositing method can be applied during all compositing period of a year (to be discussed in details in section 5). For those that did not have perennial snow/ice or surface water cover, their SCC is determined for each compositing period using the following:

$$\text{SCC}=\begin{cases}\text{condition 1}, & \text{CF}(SP_{sub-yearly} \geq T_{\text{SP}}) \geq T_{\text{CF}} \\ \textit{Not}\ \text{condition 1}, & \text{CF}(SP_{sub-yearly} \geq T_{\text{SP}}) < T_{\text{CF}}\end{cases} \quad (2)$$

Equation (2) is essentially the same as equation (1) except that CP is changed to CF (cumulative frequency). This is necessary because for short compositing periods there are only a small number of observations in each period. Frequency can represent the number of observations out of a small pool more precisely than percentage. T_{CF} is threshold of the number of observations.

3.2.4 Implementation of the SA-comp method

Based on the spectral-temporal and statistical characteristics of different SCCs under both clear-sky and cloudy/shadow conditions, the SA-comp method consists of the rules (Figure 5):

Rule 1: If more than 95% of a pixel's daily observations in a year had NDVI values below 0.2, the pixel was not vegetated throughout the year. Otherwise it had vegetation cover during at least

part of the year.

Rule 2: For a pixel that had no vegetation cover during the entire year, it was covered by snow/ice or water throughout the year if its NDWI values were negative for less than 5% of the time. The SCC remains the same for all compositing periods of the year for compositing method selection. Otherwise barren was observed during at least part of the year, and whether barren was observed during a specific compositing period needs to be determined using rule 3.

Rule 3: Since the pixel was not vegetated throughout the year and hence not vegetated during a specific compositing period, and barren was observed during at least part of a year, barren was observed during that compositing period if at least one daily observation in this period had a negative NDWI value. Otherwise barren was not observed and the pixel had snow/ice or water cover during the entire compositing period.

Rule 4: Since the pixel had vegetation cover during at least part of the year according to rule 1, it had vegetation cover in a specific period if at least one daily observation in this period had an NDVI value > 0.2. Otherwise it did not have vegetation cover during this period, and rule 3 is used to determine whether barren was observed during this period.

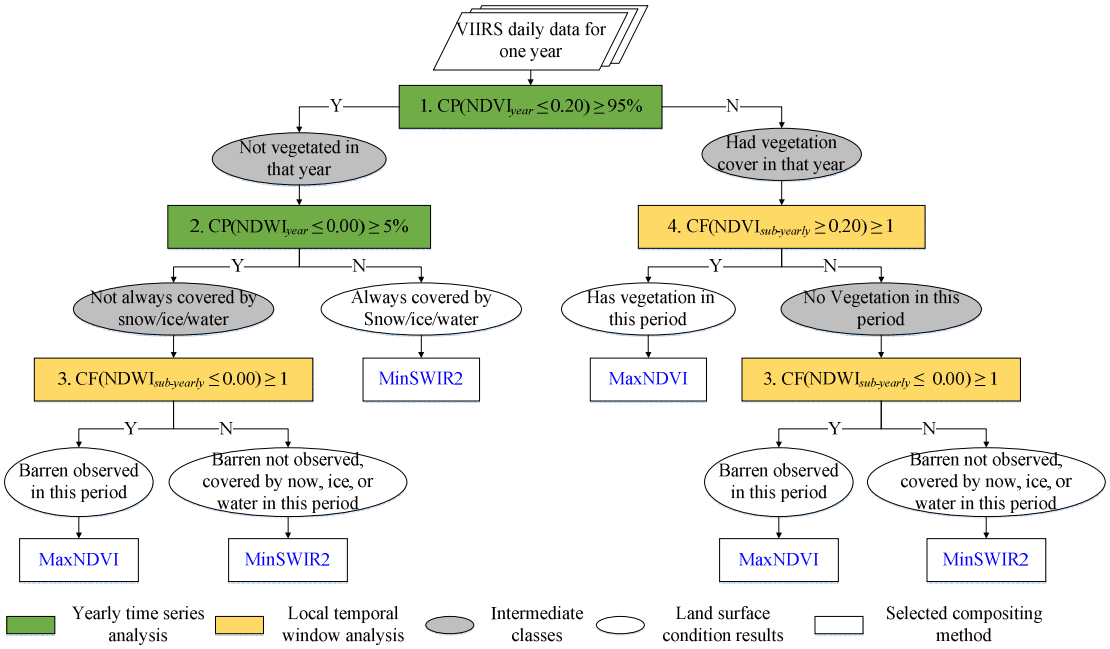

Figure 5. Structure of the SA-Comp method. The VIIRS daily data include both clear-sky observations as well as observations contaminated by clouds and cloud shadow.

Once the SCC for each compositing period is determined, an optimal compositing method can be selected for the SCC. Based on Figure 2 and previous studies (see Table 3), the MaxNDVI method is used when vegetation or barren is observed during a compositing period. Because both water and snow/ice have low reflectance in the shortwave infrared (SWIR) band (M10), a minimum SWIR method would allow identification of clear-sky observations when the surface cover is either snow/ice or water. In this study, the second minimum SWIR method (MinSWIR2) is used as there may be a low likelihood of cloud shadow, which is unlikely to occur more than once within a short compositing period. The SA-Comp method was implemented according the flowchart shown in Figure 1 for generating clear-sky global VIIRS composited images. The processing steps include reading the VIIRS daily data, calculating the relevant spectral indices, determining SCCs, selecting

the appropriate compositing method and creating the composites. These steps are repeated pixel by pixel for the entire globe.

3.3 Quality assessment

The SA-Comp method was used to create 8- and 16-day composites. The 8-day composites were compared with the MODIS Collection 6 8-day composites (MYD09A1), which were produced using the best observation method (Vermote et al., 2015), and with the VIIRS VNP09A1 products produced using a stepwise compositing scheme (Roger et al., 2016). In addition to visual assessment, we also examined the annual temporal profiles of selected samples to determine whether the desired observations were selected in each compositing period.

4. Results and Analysis

4.1 Overall quality of derived global composites

The global VIIRS composites of 2015 were generated at 8-day and 16-day time intervals using the proposed SA-Comp method. Considering the limitations on space, Fig. 6 shows the global 8-day VIIRS compositing results using a sinusoidal projection for four different seasons. The panels are false color composites with a red-green-blue (RGB) color scheme of bands M10, M7 and M5, respectively, using the same stretch.

Generally, the results evidently reveal the effectiveness of the SA-Comp method in excluding cloudy pixels from clear-sky pixels. The composites exhibit very small cloud cover percentages at the global scale. However, the Amazon basin did contain some residual cloud cover in the composites under the influence of strong precipitation, especially along the coastal region. Similarly, Southwest China also demonstrated some residual clouds in the composites under the influences of the Pacific and Indian monsoons. The geographic distribution and phenology of vegetation were evident, and the observed differences were mainly related to the timing of growth between natural and agricultural vegetation. The spatio-temporal distribution of snow was apparent, which can be observed in the high mountains and high latitudes during the winter season. Areas of barren land, including deserts (*e.g.*, the Sahara Desert) and the transition zones between barren land and sparse vegetation, were effectively distinguishable with larger red and lower green reflectance values. Overall, the dramatic contrasts between different surface types revealed by the SA-Comp composites were crucial for accurate surface type mapping and biophysical parameters retrieval at the global scale.

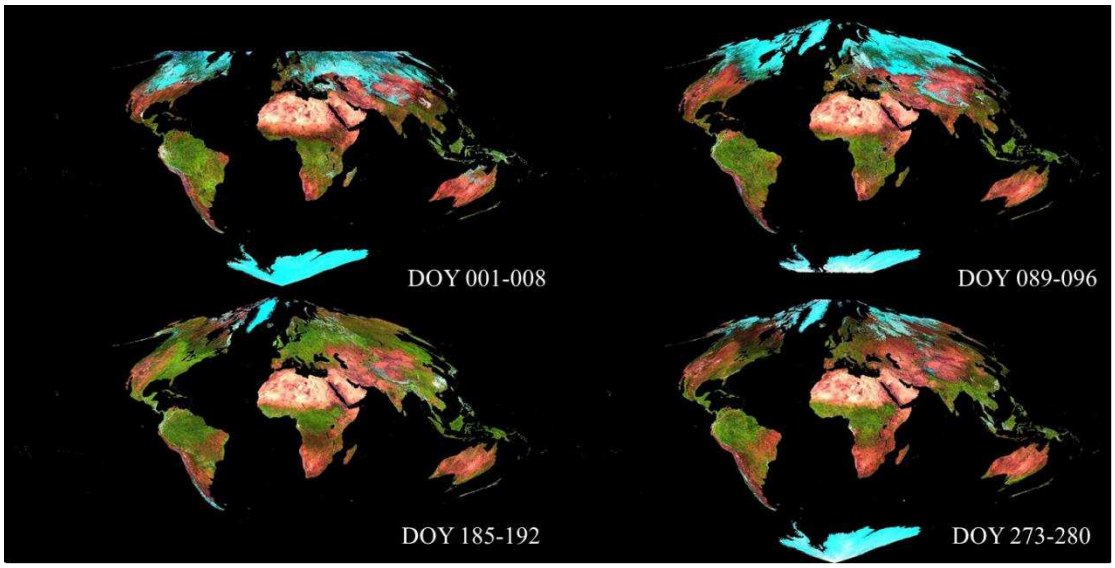

Figure 6. Example 8-day global VIIRS composites produced using the SA-Comp method for 2015 with an M10, M7, M5 RGB color scheme. DOY: day of year.

4.2 Comparisons with other compositing methods

To demonstrate the advantages of the SA-Comp method over the other methods, Fig. 7 further illustrates the enlarged details of four different methods over various land cover types. The images are false color composites with an RGB color scheme employing the M10 (as red color), M7 (as green color) and M5 (as blue color) bands using the same stretch. The surface types were mainly open water (North America), permanent snow (Greenland), barren land (Africa), and savanna (Australia). Fig. 7 (a), (b), (c), and (d) show the results acquired from the MaxNDVI, MaxRatio, MinRed, and SA-Comp compositing schemes, respectively.

Obviously, although the MaxNDVI method was able to eliminate clouds and cloud shadows over vegetated surfaces, it failed to exclude cloud contamination over open water and snow areas. The MaxRatio method performed slightly better than the MaxNDVI method over snow areas, but it was still unsuccessful at eliminating clouds over snow, open water and barren land areas. Meanwhile, the MinRed technique was very successful at eliminating clouds but introduced many cloud shadow pixels into the final composites. Because snow usually exhibits a high reflectance in the red band (often leading to a saturated signal), the MinRed method also failed at discriminating clouds over snow areas. The SA-Comp method outperformed all of the other compositing methods in each case. The comparisons above demonstrate that the SA-Comp approach significantly improves upon the existing single-criterion methods with regard to the discrimination of clouds and cloud shadows.

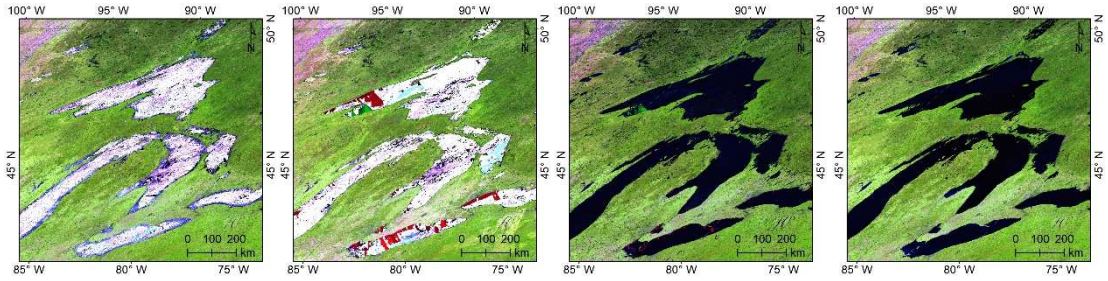

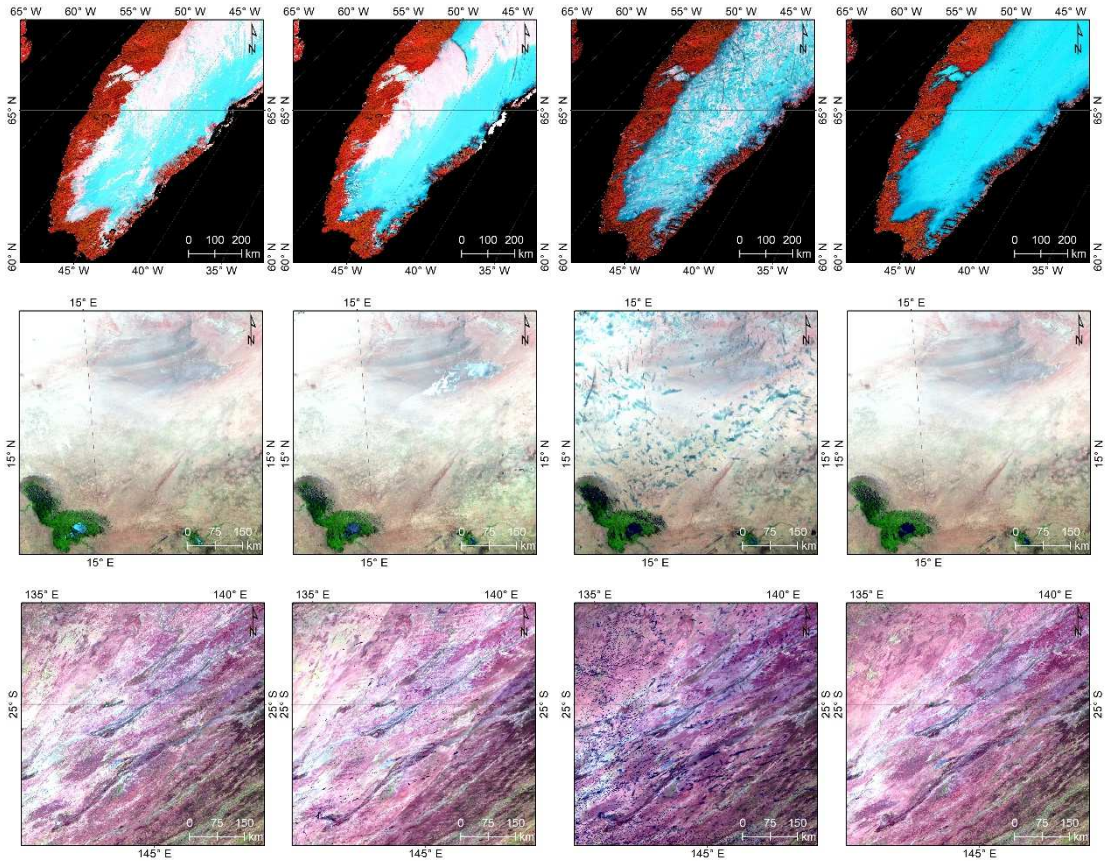

Figure 7. VIIRS 16-day composite images generated by different schemes, namely, the (a) MaxNDVI, (b) MaxRatio, (c) MinRed, and (d) proposed SA-Comp methods. The time interval is 16 days.

4.3 Comparison with existing MODIS and VIIRS composites

4.3.1 Visual effects

Both MODIS and VIIRS 8-day composited surface reflectance products were selected to compare the performance of the proposed method. A latitudinal gradient in the Northern Hemisphere from the equator to boreal Russia was selected as an example. The area also includes most of the Tibetan Plateau. As both the MODIS Aqua satellite and the NPP VIIRS satellite are situated within the same 13:00 sun-synchronous orbit, the Aqua MODIS MYD09A1 C6 product and the VIIRS VNP09A1 product were selected for comparison. The Aqua MODIS MYD09A1 product adopts the most effective observation method that selects the best conditions over the given period (Vermote et al., 2015), while the NASA NPP VIIRS product adopts a stepwise compositing scheme that considers the observational coverage and uses score-based criteria. The observations with the highest scores and lowest view angles are selected as the VNP09A1 outputs (Roger et al., 2016). Cloud mask products were used as the auxiliary data for both products.

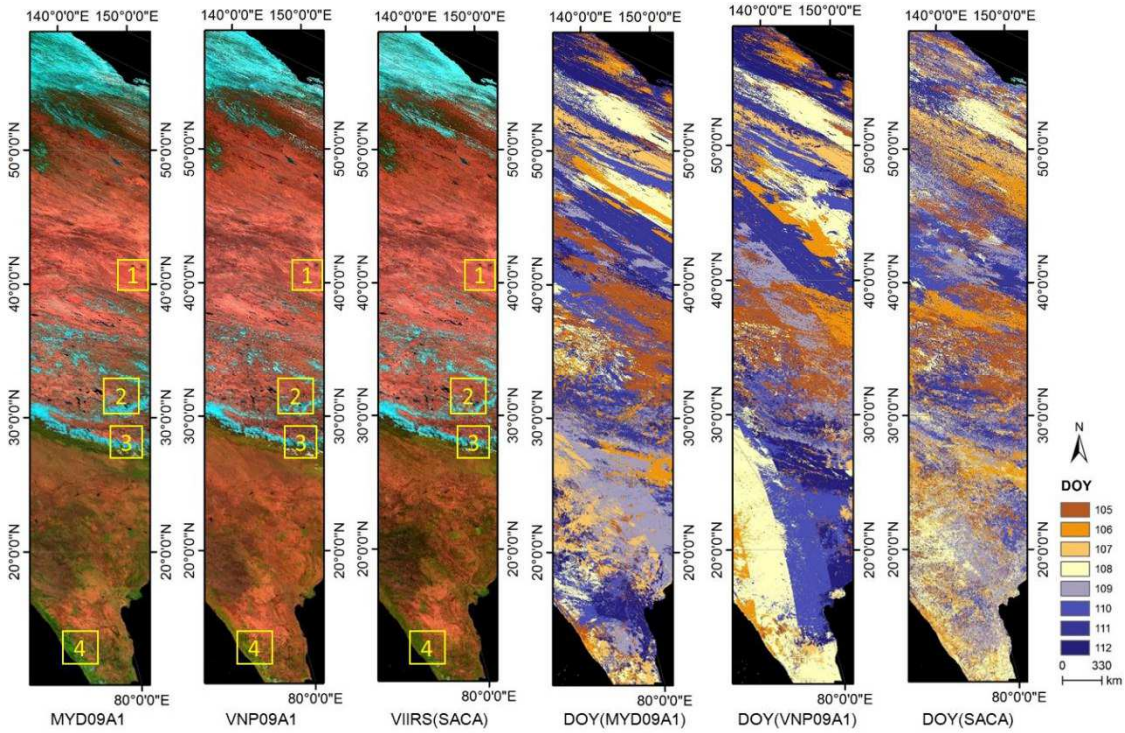

Figure 8. Comparison between the MODIS MYD09A1 and NASA VNP09A1 8-day surface reflectance products and the results from SA-Comp. The first column shows the MODIS MYD09A1 product, the second column shows the NASA NPP 8-day reflectance product, and the third column shows the results from the proposed SA-Comp method. The fourth through the sixth columns display the DOY of the corresponding products.

Fig. 8 depicts the compositing results obtained from the MYD09A1 C6 and VNP09A1 products and the SA-Comp method from DOY 105 to DOY 112 using the same stretch. Generally, the composites from the SA-Comp method were visually consistent with those from the other two products. The sub-tropical land surfaces (~23°N-60°N) were similar among all three products. However, large heterogeneities were visible in the tropical belts (~5°N-23°N) attributable to differences in the beginning dates of the growth seasons for different vegetation types. Swath boundaries were evident in both the surface reflectance and the DOY in the VNP09A1 product. These boundaries were mainly caused by the observational coverage and the angular-related criteria in the compositing scheme. A greater number of residual clouds were also observed in the VNP09A1 product. Although the SA-Comp approach did not require any cloud mask product, it is clear that SA-Comp results was more effective at excluding clouds than the VNP09A1 product.

Fig. 9 further illustrates four areas in enlarged detail. The location of each area is delineated with a yellow rectangle in Fig. 8. Following a visual inspection, the SA-Comp method outperformed the MYD09A1 and VNP09A1 products in each enlarged area with fewer residual clouds and cloud shadows. The VNP09A1 product also performed relatively well, which can be attributed to the ability of the compositing scheme to select the best pixels. However, it failed to remove some small cloud shadows and cloud patches, which were evident in the enlarged details. This further emphasizes that the use of auxiliary data (*e.g.*, cloud and cloud shadow mask products) in the compositing procedure may transfer commission and omission errors into the final compositing results. The SA-Comp method, which employed temporal information to determine the surface conditions, demonstrated apparent advantages in the compositing procedure.

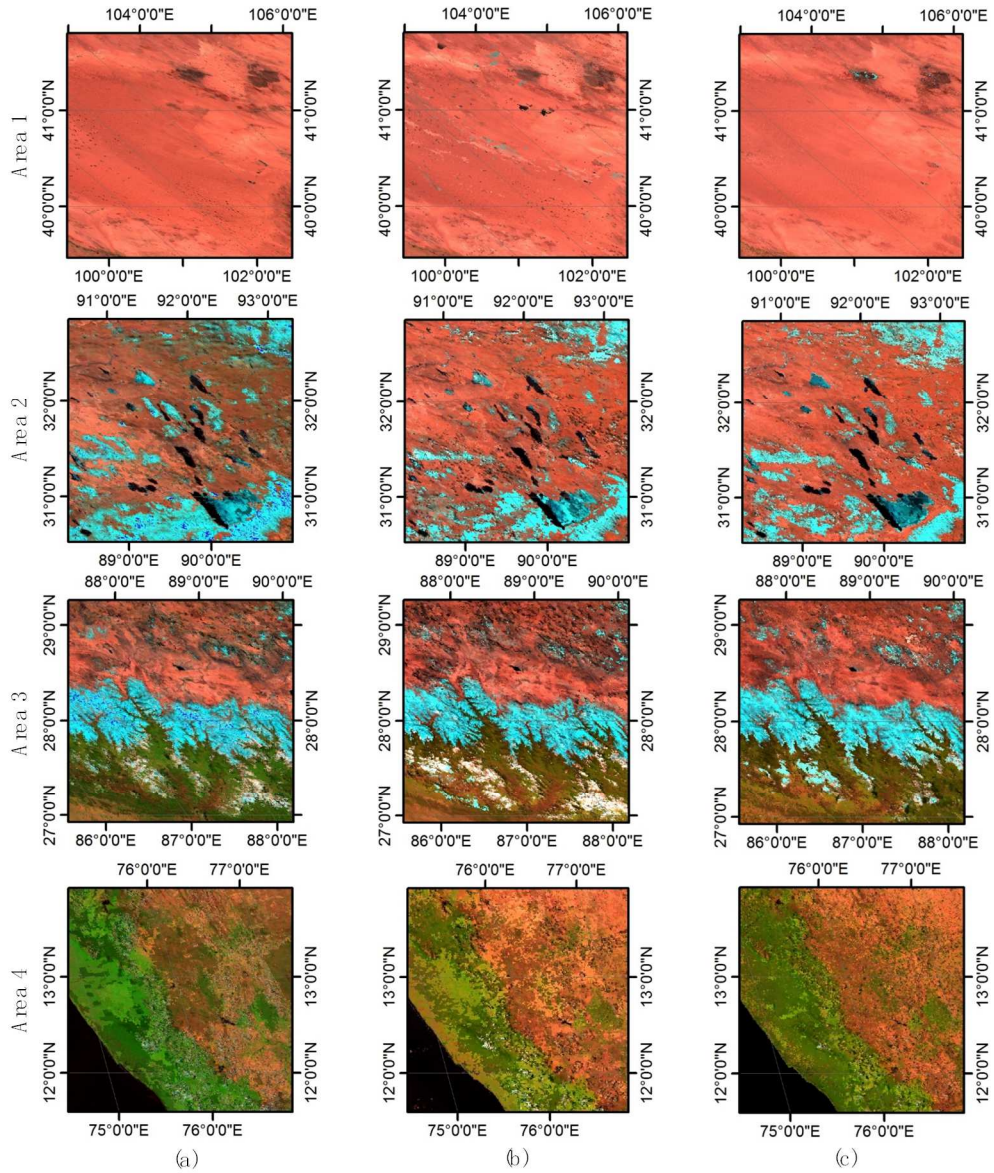

Figure 9. Enlarged details of the results from the (a) MODIS MYD09A1 and (b) NASA VIIRS VNP09A1 products and (c) SA-Comp.

4.3.2 Comparison of temporal profiles between the VNP09A1 product and SA-Comp

Fig. 10 further compares the 8-day temporal profiles from the VNP09A1 product and the SA-Comp method for four typical land cover types, namely, permanent snow, open water, cropland and barren land. The temporal profiles from the SA-Comp method were much more stable and consistent among the different surface types than those of the VNP09A1 product. For open water, the NDVI values from the VNP09A1 product were close to zero (red arrows) and the surface reflectances in the red band were very high on several days, suggesting that those days were cloudy. In contrast, the SA-Comp approach successfully captured the spectral characteristics of water on those days. The temporal profiles of permanent snow fluctuated dramatically with regard to the NDSI profile and the SWIR band, indicating that the VNP09A1 product contained more noisy signals than the SA-Comp method. Steep rises and sudden drops in the VNP09A1 profiles for desert and evergreen vegetation also demonstrate that those pixels were incorrectly selected.

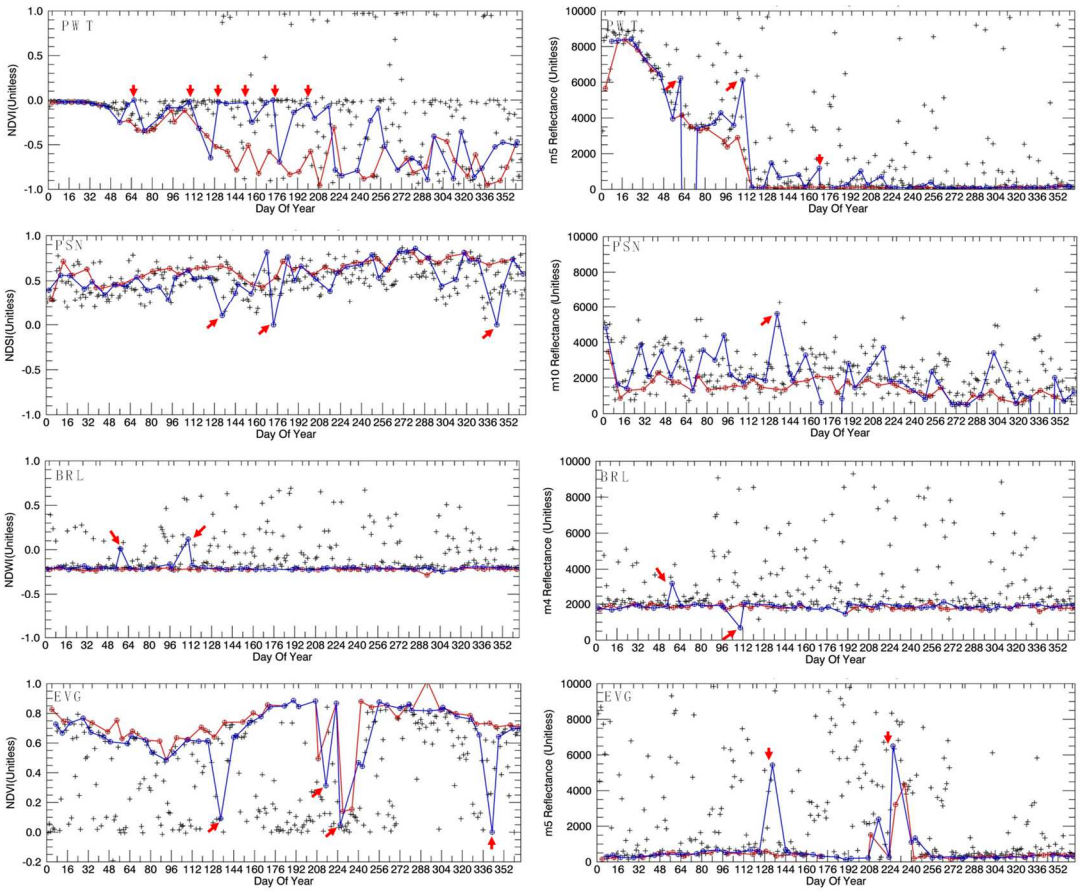

Figure 10. Comparison of the temporal profiles between SA-Comp and the VNP09A1 product for typical surface types. The red lines show the compositing results of the SA-Comp method, the blue lines depict the 8-day compositing products from the VNP09A1 product, and the black crosses show the daily surface reflectance or spectral index values.

5. Discussion

Spectrally consistent and spatio-temporally continuous time series remote sensing images are significant for many Earth system studies (Bian et al., 2017; Huang et al., 2009; Roy et al., 2010). However, due to frequent cloud contamination and poor atmospheric conditions, daily remote sensing images are usually spatially and temporally discontinuous (Pede and Mountrakis, 2018; Pringle et al., 2009). Image compositing is a popular technique that can be utilized to select the most representative pixel over the same geographical region from multi-temporal images in a certain time window, and it can increase the spatio-temporal continuity of time series images (Bian et al., 2015; Griffiths et al., 2013; Luo et al., 2008). A critical challenge in image compositing is selecting the most suitable compositing rules for different surface types, especially when being implemented at the global scale. Currently, only a few studies have used temporal information in the temporal compositing procedure, especially with VIIRS image products (Frantz et al., 2017; Jiang et al., 2016). Conversely, this study proposed a new SA-Comp approach that uses using temporal information to determine the SCCs and generate cloud-free VIIRS composites. While some studies have compared the advantages of different compositing methods for generating cloud-free composites (Lück and van Niekerk, 2016), the SA-Comp approach suggests that contextual temporal and spectral information can be effectively used by considering the characteristics at both

the annual and the sub-yearly temporal scales during the image compositing procedure.

The SA-Comp approach implements a self-adaptive scheme to automatically select the most suitable compositing criterion for a given SCC during a specific compositing period. Its performance was tested using daily VIIRS surface reflectance product for 2015 and compared with three compositing methods, namely, the MinRed, MaxNDVI and MaxRatio methods. Each of the four methods was used to generate 8-day and 16-day VIIRS composites. The MODIS MYD09A1 and VIIRS VNP09A1 products, which represent products derived using a best observation method (Vermote et al., 2015) and a stepwise compositing scheme (Roger et al., 2016), respectively, were also used for comparison. Despite the similar visual results from the SA-Comp approach and the other single-criterion compositing methods, substantial differences were observed in the enlarged composites (Fig. 7). The MaxNDVI method is suitable for compositing over vegetated areas, but it does not work when the vegetation cover is replaced by snow/ice in the wintertime or by water due to flood. Minimum methods are more effective for cloud screening over surfaces covered by snow/ice or water, though they also tend to prefer cloud shadows when they are present (Lück and van Niekerk, 2016). The SA-Comp method implements a self-adaptive approach for choosing between the MaxNDVI and MinSWIR2 criteria based on the SCC at a given pixel location during a specific compositing period. Overall, it produced desirable results at both local and global scales. Some SA-Comp results had residual clouds and cloud shadows that did not form large connected areas. These could result from lack of any clear-sky observation over those areas during the concerned compositing period, or be errors from the MinSWIR2 method when there was only one clear-sky observation (Zhang et al., 2017).

The proposed SA-Comp approach in this paper is simple and easily implemented. Unlike the compositing methods used for most remote sensing products such as MYD09A1 and VNP09A1, the SA-Comp approach in this paper does not depend on a cloud mask product. It uses spectral and temporal information to determine the SCCs based on which an appropriate compositing method is selected. If available, a cloud mask product may be used to improve this method, even such a product inevitably contain some uncertainties (Justice et al., 2013; Sun et al., 2017). Further improvements might be achieve by using additional bands or spectral indices. For example, it has been well established that thermal bands can be used to improve cloud detection (Huang et al., 2010). Other spectral indices like enhanced vegetation index (EVI) (Huete et al., 2002) and the normalized difference phenology index (NDPI) (Wang et al., 2017) may provide useful information for determining the SCCs in addition to the three indices used in this study. Currently, the SCCs in each compositing period are outputted with the final composites. However, As SCCs is only the surface cover status in the compositing period, it cannot provide enough quality information of the composites for the users. In future works, whether each observation is cloudy will be further identified using the clear-sky composites. The quality control data layer containing number of clear-sky observations in the compositing period, the quality of each observation (*e.g.*, clear-sky or cloudy) and the quality of the composites (*e.g.*, clear-sky or residual clouds) will be provided for quantitative and qualitative applications of the composites.

The performance of the SA-Comp method does not depend on high levels of thematic details or extremely high accuracies in determining the SCCs. In fact, although the algorithm can separate barren from vegetation cover (Figure 5), it uses the same MaxNDVI method to composite for both SCCs. Similarly, Figure 2 shows that both M5 and M7 can be used to separate water from snow/ice. But there is no need to do this as the MinSWIR2 method is effective for both SCCs. Confusions

between vegetation and snow/ice or between vegetation and water is unlikely unless a pixel is a mixed pixel. In such a case either the MaxNDVI or MinSWIR2 should work because they will choose clear-sky observations over cloudy ones. Similarly, confusions between water and barren or snow/ice and barren are most likely due to mixed SCCs in a pixel. Again such confusions do not necessarily result in errors in the composited results. While the SA-Comp method assumes that the SCC at a pixel location does not change during a specific compositing period (section 3.2.3), which may not be always true, violation of this assumption does not necessarily lead to erroneous results either. For example, if a barren area was flooded and changed to water during a compositing period, the SCC for compositing method selection should depend on which of the two SCCs was observed under clear-sky conditions, and the selected compositing method should choose a clear-sky observation over cloudy ones.

The SA-Comp method uses one full year's archived daily surface reflectance data as input. While this can be a burden for near-real-time compositing as it requires more computing resources, it should contribute to improved efficiency because for pixels that have the same SCC throughout a year the SCC only needs to be determined once, not for every compositing period. The SCC determined using a large number of observations acquired in a year should also be more reliable than that determined based on a few observations available within a compositing period.

The SA-Comp approach has been tested using 2015 global surface reflectance data acquired by VIIRS onboard the S-NPP satellite. VIIRS is also onboard the recently launched JPSS1 and will be deployed on future JPSS satellites. This algorithm should be directly applicable to data acquired by these new VIIRS instruments. It likely can be adapted for use with other global observation systems such as MODIS and Sentinel-3 after applying necessary adjustments. It might also be adapted for use with fine-resolution systems such as Landsat 8, Sentinel-2, and HJ-1A/B (Huanjing (HJ), which means environment in Chinese) to produce fine-resolution global composites; this hypothesis will be pursued in our future work. At such fine spatial resolutions, however, spectral topographic distortions in mountainous areas can be significant and need to be considered (Li et al., 2012; Li et al., 2015).

6. Conclusions

This study proposed an effective and practical SA-Comp approach for compositing clear-sky VIIRS surface reflectance data by adapting the compositing process to the land surface phenology of each pixel. The proposed approach consists of a new multi-temporal analysis method for automatically determining the surface cover conditions (SCCs) and the appropriate compositing criteria most suitable different SCCs. The feasibility and effectiveness of the proposed approach were assessed and confirmed by comparing the compositing results from the SA-Comp with those from different compositing methods and from MODIS and VIIRS compositing products.

The results demonstrated that the SA-Comp approach was more efficient and accurate than the MaxNDVI, MinRed and MaxRatio methods. A comparison of the temporal profiles obtained using SA-Comp with the VNP09A1 product revealed that the SA-Comp composites could accurately depict the detailed temporal variations on the ground in both time and space.

Given the demonstrated efficiency and effectiveness of the SA-Comp approach, it will be used to produce global VIIRS composites for other years. Efforts will also be made to adapt it for use with other global observing systems like MODIS and Sentinel-3, and for use at fine (30 m or finer) spatial resolutions.

Acknowledgements

This research was jointly funded by the Strategic Priority Research Program of the Chinese Academy of Sciences (CAS) (XDA19030303), the National Natural Science Foundation project of China (41701432, 41631180, 41571373), the National Key Research and Development Program of China (No. 2016YFA0600103, 2016YFC0500201-06), the 135 Strategic Program of the Institute of Mountain Hazards and Environment, CAS (SDS-135-1708), the CAS "Light of West China" Program, the Youth Talent Team Program of Institute of Mountain Hazards and Environment, CAS (SDSQB-2015-02), and the Joint Polar Satellite System (JPSS) program of the National Oceanic and Atmospheric Administration (NOAA). We are grateful to the anonymous reviewers for their many valuable comments and suggestions that helped improve the manuscript.

References

Bian, J., Li, A., Wang, Q., Huang, C., 2015. Development of Dense Time Series 30-m Image Products from the Chinese HJ-1A/B Constellation: A Case Study in Zoige Plateau, China. Remote sens., 7, 16647-16671.

Bian, J., Li, A., Zhang, Z., Zhao, W., Lei, G., Yin, G., Jin, H., Tan, J., Huang, C., 2017. Monitoring fractional green vegetation cover dynamics over a seasonally inundated alpine wetland using dense time series HJ-1A/B constellation images and an adaptive endmember selection LSMM model. Remote Sens. Environ. 197, 98-114.

Cabral, A., De Vasconcelos, M.J.P., Pereira, J.M.C., Bartholome, E., Mayaux, P., 2003. Multi-temporal compositing approaches for SPOT-4 VEGETATION. International Journal of Remote Sensing 24, 3343-3350.

Cao, C.Y., Xiong, J., Blonski, S., Liu, Q.H., Uprety, S., Shao, X., Bai, Y., Weng, F.Z., 2013. Suomi NPP VIIRS sensor data record verification, validation, and long-term performance monitoring. J. Geophys. Res-Atmos., 118.

Chuvieco, E., Ventura, G., Martin, M.P., Gomez, I., 2005. Assessment of multitemporal compositing techniques of MODIS and AVHRR images for burned land mapping. Remote Sens. Environ., 94, 450-462.

Dennison, P.E., Roberts, D.A., Peterson, S.H., 2007. Spectral shape-based temporal compositing algorithms for MODIS surface reflectance data. Remote Sens. Environ., 109, 510-522.

Flood, N., 2013. Seasonal Composite Landsat TM/ETM plus Images Using the Medoid (a Multi-Dimensional Median). Remote Sens., 5, 6481-6500.

Frantz, D., Röder, A., Stellmes, M., Hill, J., 2017. Phenology-adaptive pixel-based compositing using optical earth observation imagery. Remote Sens. Environ., 190, 331-347.

Gao, B.-C., 1996. NDWI—A normalized difference water index for remote sensing of vegetation liquid water from space. Remote Sens. Environ., 58, 257-266.

Griffiths, P., van der Linden, S., Kuemmerle, T., Hostert, P., 2013. Pixel-Based Landsat Compositing Algorithm for Large Area Land Cover Mapping. IEEE J-STARS 6, 2088-2101.

Hall, D.K., Riggs, G.A., Salomonson, V.V., 1995. Development of methods for mapping global snow cover using moderate resolution imaging spectroradiometer data. Remote Sens. Environ., 54, 127-140.

Higginbottom, T.P., Symeonakis, E., Meyer, H., van der Linden, S., 2018. Mapping fractional woody cover in semi-arid savannahs using multi-seasonal composites from Landsat data. ISPRS J. Photogramm. Remote Sens., 139, 88-102.

Hillger, D., Kopp, T., Lee, T., Lindsey, D., Seaman, C., Miller, S., Solbrig, J., Kidder, S., Bachmeier, S., Jasmin, T., Rink, T., 2013. First-Light Imagery from Suomi NPP VIIRS. B. Am. Meteorol. Soc., 94, 1019-1029.

Holben, B.N., 1986. Characteristics of Maximum-Value Composite Images from Temporal AVHRR Data. International Journal of Remote Sensing, 7, 1417-1434.

Huang, C.Q., Goward, S.N., Masek, J.G., Gao, F., Vermote, E.F., Thomas, N., Schleeweis, K., Kennedy, R.E., Zhu, Z.L., Eidenshink, J.C., Townshend, J.R.G., 2009. Development of time series stacks of Landsat images for reconstructing forest disturbance history. Int. J. Digit Earth, 2, 195-218.

Huang, C.Q., Thomas, N., Goward, S.N., Masek, J.G., Zhu, Z.L., Townshend, J.R.G., & Vogelmann, J.E., 2010. Automated masking of cloud and cloud shadow for forest change analysis using Landsat images. International Journal of Remote Sensing, 31, 5449-5464

Huete, A., Didan, K., Miura, T., Rodriguez, E.P., Gao, X., Ferreira, L.G., 2002. Overview of the radiometric and biophysical performance of the MODIS vegetation indices. Remote Sens. Environ., 83, 195-213.

Jiang, Z., Vargas, M., Csiszar, I., 2016. New oprational real-time daily rolling weekly Green Vegetation fraction product derived from suomi NPP VIIRS reflectance data, 2016 IEEE International Geoscience and Remote Sensing Symposium (IGARSS), pp. 3524-3527.

Justice, C.O., Roman, M.O., Csiszar, I., Vermote, E.F., Wolfe, R.E., Hook, S.J., Friedl, M., Wang, Z.S., Schaaf, C.B., Miura, T., Tschudi, M., Riggs, G., Hall, D.K., Lyapustin, A.I., Devadiga, S., Davidson, C., Masuoka, E.J., 2013. Land and cryosphere products from Suomi NPP VIIRS: Overview and status. J. Geophys. Res-Atmos., 118, 9753-9765.

Li, A., Jiang, J., Bian, J., Deng, W., 2012. Combining the matter element model with the associated function of probability transformation for multi-source remote sensing data classification in mountainous regions. ISPRS J. Photogramm. Remote Sens., 67, 80-92.

Li, A., Wang, Q., Bian, J., Lei, G., 2015. An Improved Physics-based Model for Topographic Correction of Landsat TM Images. Remote sens., 7, 6296-6319.

Lück, W., van Niekerk, A., 2016. Evaluation of a rule-based compositing technique for Landsat-5 TM and Landsat-7 ETM+ images. International Journal of Applied Earth Observation and Geoinformation 47, 1-14.

Luo, Y., Trishchenko, A.P., Khlopenkov, K.V., 2008. Developing clear-sky, cloud and cloud shadow mask for producing clear-sky composites at 250-meter spatial resolution for the seven MODIS land bands over Canada and North America. Remote Sens. Environ., 112, 4167-4185.

Niclòs, R., Pérez-Planells, L., Coll, C., Valiente, J.A., Valor, E., 2018. Evaluation of the S-NPP VIIRS land surface temperature product using ground data acquired by an autonomous system at a rice paddy. ISPRS J. Photogramm. Remote Sens., 135, 1-12.

NOAA, 2014. Joint Polar Satellite System (JPSS) VIIRS Surface Reflectance Algorithm Theoretical Basis Document (ATBD), NOAA. https://www.star.nesdis.noaa.gov/jpss/documents/ATBD/D0001-M01-S01-026_JPSS_ATBD_VIIRS-Surface-Reflectance_A.pdf (accessed on 20 June 2018)

NOAA, 2016. NOAA's Comprehensive Large Array-Data Stewardship System. http://www.class.noaa.gov/ (accessed on 20 June 2018)

Pede, T., Mountrakis, G., 2018. An empirical comparison of interpolation methods for MODIS 8-day land surface temperature composites across the conterminous Unites States. ISPRS J. Photogramm. Remote Sens., 142, 137-150.

Pringle, M.J., Schmidt, M., Muir, J.S., 2009. Geostatistical interpolation of SLC-off Landsat ETM+

images. ISPRS J. Photogramm. Remote Sens., 64, 654-664.
Roger, J.C., Vermote, E.F., Devadiga, S., Ray, J.P., 2016. Suomi-NPP VIIRS Surface Reflectance User's Guide V1 Re-processing (NASA Land SIPS). (https://lpdaac.usgs.gov/sites/default/files/public/product_documentation/vnp09_user_guide.pdf). (accessed on 20 June 2018)
Roy, D.P., Ju, J.C., Kline, K., Scaramuzza, P.L., Kovalskyy, V., Hansen, M., Loveland, T.R., Vermote, E., Zhang, C.S., 2010. Web-enabled Landsat Data (WELD): Landsat ETM plus composited mosaics of the conterminous United States. Remote Sens. Environ, 114, 35-49.
Sun, L., Mi, X., Wei, J., Wang, J., Tian, X., Yu, H., Gan, P., 2017. A cloud detection algorithm-generating method for remote sensing data at visible to short-wave infrared wavelengths. ISPRS J. Photogramm. Remote Sens., 124, 70-88.
Tucker, C.J., 1979. Red and photographic infrared linear combinations for monitoring vegetation. Remote Sens. Environ., 8, 127-150.
Vermote, E., Vermeulen, A., 1999. Atmospheric correction algorithm: spectral reflectances (MOD09). ATBD version 4.
Vermote, E.F., Roger, J.C., Ray, J.P., 2015. MODIS Surface Reflectance User's Guide Collection 6.
Wang, C., Chen, J., Wu, J., Tang, Y.H., Shi, P.J., Black, T.A., Zhu, K., 2017. A snow-free vegetation index for improved monitoring of vegetation spring green-up date in deciduous ecosystems. Remote Sens. Environ., 196, 1-12.
Zhang, R., Huang, C., Zhan, X., Jin, H., Song, X.-P., 2017. Development of S-NPP VIIRS global surface type classification map using support vector machines. Int. J. Digit Earth, 1-21.